PIEZO2 mediates ultrasonic hearing via cochlear outer hair cells in mice

Jie Li[a,b,1], Shuang Liu[a,b,1], Chenmeng Song[a,b,1], Qun Hu[a,b,1], Zhikai Zhao[a,b,1], Tuantuan Deng[b,c,d], Yi Wang[a,b], Tong Zhu[a,b], Linzhi Zou[a,b], Shufeng Wang[a,b], Jiaofeng Chen[a,b], Lian Liu[a,b], Hanqing Hou[a,b], Kexin Yuan[a,e], Hairong Zheng[f], Zhiyong Liu[g], Xiaowei Chen[h,i], Wenzhi Sun[j,k], Bailong Xiao[b,c,d], and Wei Xiong[a,b,2]

[a]School of Life Sciences, Tsinghua University, Beijing, China 100084; [b]IDG (International Data Group)/McGovern Institute for Brain Research at Tsinghua University, Tsinghua University, Beijing, China 100084; [c]School of Pharmaceutical Sciences, Tsinghua University, Beijing, China 100084; [d]Tsinghua-Peking Joint Center for Life Sciences, Tsinghua University, Beijing, China 100084; [e]Department of Biomedical Engineering, School of Medicine, Tsinghua University, Beijing, China 100084; [f]Paul C. Lauterbur Research Center for Biomedical Imaging, Shenzhen Key Laboratory for MRI, Shenzhen Institutes of Advanced Technology, Chinese Academy of Sciences, Shenzhen, China 440305; [g]Institute of Neuroscience, CAS (Chinese Academy of Sciences) Center for Excellence in Brain Science and Intelligence Technology, Shanghai Institutes for Biological Sciences, Chinese Academy of Sciences, Shanghai, China 200031; [h]Brain Research Center and State Key Laboratory of Trauma, Burns, and Combined Injury, Third Military Medical University, Chongqing, China 400038; [i]CAS (Chinese Academy of Sciences) Center for Excellence in Brain Science and Intelligence Technology, Shanghai Institutes for Biological Sciences, Chinese Academy of Sciences, Shanghai, China 200031; [j]Chinese Institute for Brain Research, Beijing, China 102206; and [k]School of Basic Medical Sciences, Capital Medical University, Beijing, China 100069

Edited by Gene E. Robinson, University of Illinois at Urbana–Champaign, Urbana, IL, and approved June 8, 2021 (received for review January 20, 2021)

Ultrasonic hearing and vocalization are the physiological mechanisms controlling echolocation used in hunting and navigation by microbats and bottleneck dolphins and for social communication by mice and rats. The molecular and cellular basis for ultrasonic hearing is as yet unknown. Here, we show that knockout of the mechanosensitive ion channel PIEZO2 in cochlea disrupts ultrasonic- but not low-frequency hearing in mice, as shown by audiometry and acoustically associative freezing behavior. Deletion of *Piezo2* in outer hair cells (OHCs) specifically abolishes associative learning in mice during hearing exposure at ultrasonic frequencies. Ex vivo cochlear Ca^{2+} imaging has revealed that ultrasonic transduction requires both PIEZO2 and the hair-cell mechanotransduction channel. The present study demonstrates that OHCs serve as effector cells, combining with PIEZO2 as an essential molecule for ultrasonic hearing in mice.

PIEZO2 | hearing | ultrasonic vocalization | mechanotransduction | hair cells

Some animals use ultrasonic hearing and vocalization to communicate and navigate in daily life (1). For example, mice vocalize at frequencies >25 kHz with intensities from 60 to 100 dB SPL (sound pressure level) during certain social behaviors, including mother–pup interactions, male–male encounters, and male–female courtship (2–4). Thus, ultrasound-based auditory communication is critical for the survival and reproduction of mice. Animal models using mice, bats, cats, and guinea pigs have provided neurophysiological insights into ultrasonic hearing (5–9). However, the precise molecular identity and cell type defining ultrasonic transduction are not known. Current scientific thought postulates that ultrasonic hearing shares well-recognized general molecular and cellular mechanisms that produce auditory transduction (10–13). However, the paucity of scientific evidence in this area of hearing research relegates these theories to unproven speculation.

Recently, it has been reported that the mechanosensitive ion channel PIEZO2 plays a critical role in the somatosensory system, including gentle touch, itch, tactile pain, proprioception, breath, and blood pressure (14, 15). Structural and functional analyses of PIEZO2 have shown that it can respond to different forms of mechanical stimuli, such as indentation and stretching (16, 17). Interestingly, PIEZO2 was found expressed at the apical surface also known as the cuticular plate of cochlear hair cells, mainly in outer hair cells (OHCs) (18). It mediates a stretch-activated current known as the reverse-polarity current in neonatal mice and is controlled by intracellular Ca^{+2} concentration (18, 19). However, this electrical current gradually reduces with age and finally disappears at approximately postnatal 7 d (P7) (19, 20), which is opposite the maturation of hair-cell mechanotransduction current (19, 21). In adult mice, knockout (KO) of *Piezo2* in the inner ear only slightly affects hearing from 8 to 20 kHz, as demonstrated by auditory brainstem response (ABR) recordings (18). To date, the physiological role of PIEZO2 in hearing is still not established (20).

In this study, we explored the role of PIEZO2 in ultrasonic hearing from a variety of KO and conditional KO (cKO) mouse lines, using ultrasonically combined approaches, including ABR recordings, behavior tests, and ex vivo cochlear imaging assays. We found that the expression of PIEZO2 in the OHCs is essential for ultrasonic hearing in mice.

Results

The Mechanosensitive Channel PIEZO2 Is Required for Ultrasonic Hearing. To evaluate ultrasonic hearing physiologically, we improved the basic ABR recordings by attaching the electrode directly to the skull bone positioned posterior to Bregma sutures

Significance

Some animals have evolved an adaptive ability for vocalizing and hearing ultrasonic frequencies that are inaudible to humans (>20 kHz). For decades, it has been postulated that animals hear ultrasonic frequencies with cochlear hair cells using an identical set of mechanotransduction molecules in the hair bundles for hearing audible frequencies. Here, we show that mice lacking mechanosensitive PIEZO2 ion channels have difficulty hearing at ultrasonic frequencies but remain remarkably sensitive to audible frequencies. Thus, animals may use a partially different mechanism for sensing ultrasonic sound emissions.

Author contributions: J.L., S.L., C.S., Q.H., Z.Z., and W.X. designed research; J.L., S.L., C.S., Q.H., Z.Z., T.D., T.Z., L.Z., S.W., J.C., L.L., and H.H. performed research; T.D., K.Y., H.Z., Z.L., X.C., W.S., and B.X. contributed new reagents/analytic tools; J.L., S.L., C.S., Q.H., Z.Z., Y.W., T.Z., and W.X. analyzed data; and J.L., S.L., C.S., Y.W., B.X., and W.X. wrote the paper.

The authors declare no competing interest.

This article is a PNAS Direct Submission.

See online for related content such as Commentaries.

[1]J.L., S.L., C.S., Q.H., and Z.Z. contributed equally to this work.

[2]To whom correspondence may be addressed. Email: wei_xiong@tsinghua.edu.cn.

This article contains supporting information online at https://www.pnas.org/lookup/suppl/doi:10.1073/pnas.2101207118/-/DCSupplemental.

Published July 8, 2021.

(−7 mm AP [anteroposterior], 0 mm ML [mediolateral]) (Fig. 1*A*, *Materials and Methods*, and *SI Appendix*, Fig. S1) and named the procedure modified ABR (mABR) recording. The mABR configuration enhances the detection stability and sensitivity to stimuli at frequencies >12 kHz in C57BL/6 (B6) mice (Fig. 1 *B* and *C*). Although ultrasonic responses were not as strong as those induced by low frequencies, the mABR waveforms induced by ultrasonic frequencies were readily distinguishable for determining

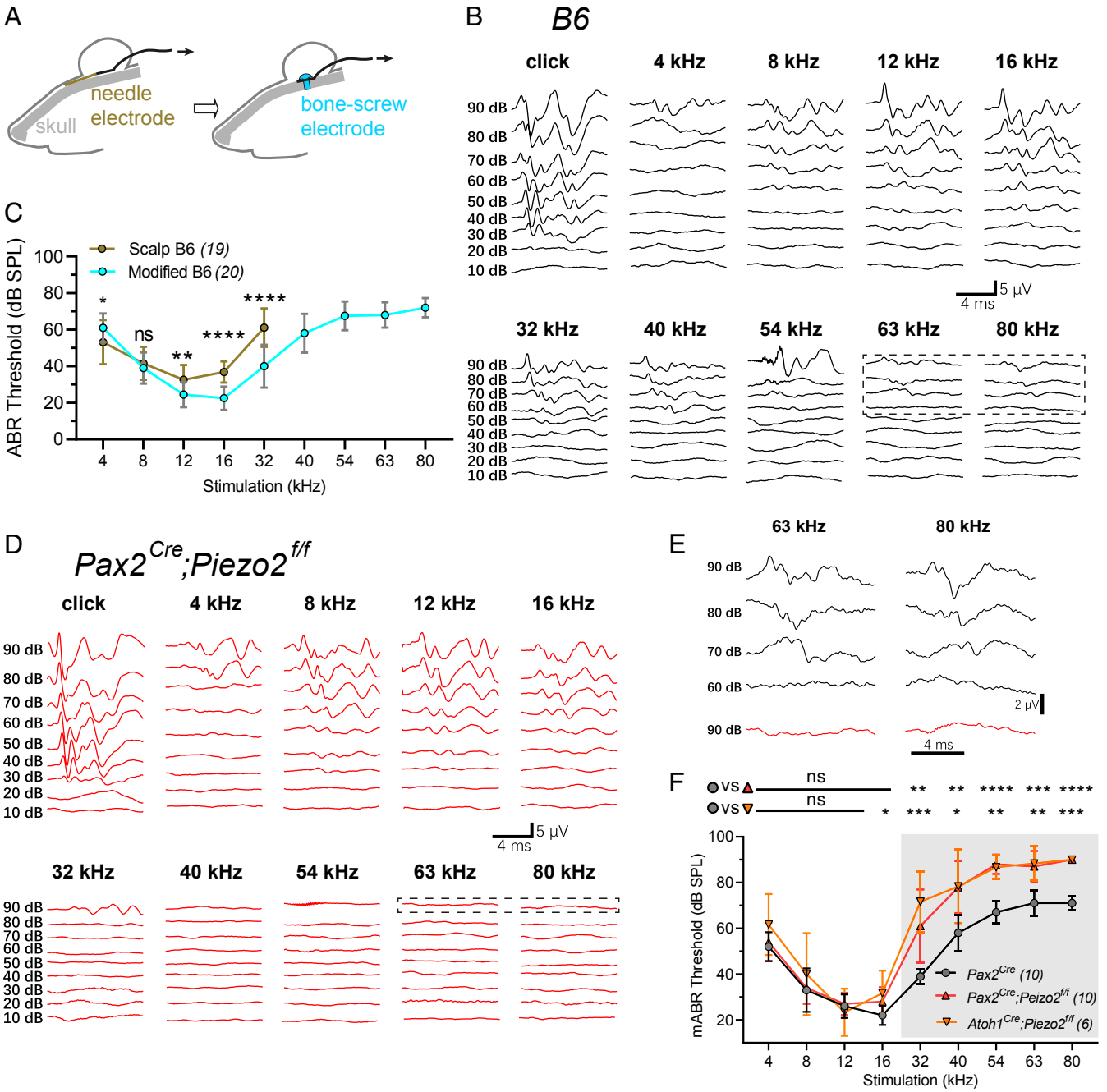

Fig. 1. The mechanosensitive channel PIEZO2 is required for ultrasonic hearing. (*A*) Schematic of recording configuration of mABR. For mABR, the recording wire was directly implanted on the mouse skull (cyan) instead of placing a needle electrode under scalp (dark yellow) (reference *SI Appendix*, Fig. S1). (*B*) Representative example of mABR signals in a C57BL/6J (B6) mouse. (*C*) Comparison of regular ABR in B6 mice with attached electrode under scalp (scalp B6, dark yellow); in B6 mice, the mABR achieved improved sensitivity to frequencies >12 kHz (modified B6, cyan). Threshold of scalp B6 and modified B6 were compared by Mann–Whitney *U* test at each frequency, 4 kHz, $^{*}P = 0.0146$; 8 kHz, $P = 0.4432$ (no significance, ns); 12 kHz, $^{**}P = 0.0028$; 16 kHz, $^{****}P < 0.0001$; 32 kHz, $^{****}P < 0.0001$. (*D*) Representative example of mABR signals in *Piezo2*-cKO mouse. (*E*) Enlarged traces with 63 and 80 kHz sound stimuli framed in *B* and *D*. (*F*) Pure-tone mABR thresholds in control *Pax2*^{Cre} mice and *Piezo2*-cKO mice. The control- and *Piezo2*-cKO mice showed distinct ABR thresholds at ultrasonic frequencies (gray-shaded area). Kruskal–Wallis test was used to compare the three groups at each frequency. *Pax2*^{Cre} mice versus *Pax2*^{Cre};*Piezo2*$^{f/f}$ cKO mice, 4 kHz, $P > 0.9999$; 8 kHz, $P > 0.9999$; 12 kHz, $P > 0.9999$; 16 kHz, $^{*}P = 0.0214$; 32 kHz, $^{***}P = 0.0022$; 40 kHz, $^{**}P = 0.0057$; 54 kHz, $^{****}P < 0.0001$; 63 kHz, $^{****}P = 0.0008$; 80 kHz, $^{****}P < 0.0001$. *Pax2*^{Cre} mice versus *Atoh1*^{Cre};*Piezo2*$^{f/f}$ cKO mice, 4 kHz, $P = 0.122$; 8 kHz, $P = 0.956$; 12 kHz, $P = 0.8272$; 16 kHz, $^{*}P = 0.025$; 32 kHz, $^{***}P = 0.0002$; 40 kHz, $^{*}P = 0.0167$; 54 kHz, $^{**}P = 0.0017$; 63 kHz, $^{**}P = 0.0026$; 80 kHz, $^{****}P = 0.0002$. All mice were recorded at ~1 mo old. For *C* and *F*, data are presented as mean ± SD, and N numbers are shown in panels.

thresholds (Fig. 1*B*). The generally decreased mABR amplitude at 63 and 80 kHz implies less efficient ultrasonic transduction at the cochlear level. This is because the ABR waveforms reflect signals from the auditory nerves that innervate the cochlear hair cells and their ascending auditory pathways (22). The 54-kHz 90 dB SPL mABR signal showed an abruptly large amplitude (Fig. 1*B*). This is consistent with previous measurements of mouse hearing, using audiometry (23) and auditory nerve recordings (24), which showed two sensitivity peaks at 15 and 55 kHz, respectively. This phenomenon was not due to distortions delivered by the speakers at high intensities, since the measured ultrasonic pure-tone output was quite condensed even at 90 dB SPL (*SI Appendix*, Fig. S1*D*).

Since *PIEZO2* pan-KO mice exhibit embryonic lethality (25), we crossed certain Cre mice with *Piezo2*$^{f/f}$ mice (26) to generate *Piezo2*-cKO mice. These mice were mainly of B6- and some mixed genetic background (*SI Appendix*, Table S1). It has been shown that mice with different backgrounds have different ultrasonic hearing sensitivities. For example, the CBA/J (CBA) mice have better ultrasonic hearing sensitivity compared to B6 mice according to the auditory nerve recordings (8 to 16 wk animals) (24) and ABR recordings (16 to 18 wk animals) (27). In addition, B6 mice exhibit progressive hearing loss late in life (>7 mo) (28, 29). To avoid the possible statistical confound of mixed genetic background in the evaluation of ultrasonic hearing, we compared the mABR sensitivity between the B6 mice and the CBA mice at ~1 mo old. This is the age at which they possess matured auditory function, occurring well before age-related hearing loss begins. The mABR recordings showed that ultrasonic hearing in B6 mice is as sensitive as that of CBA mice at the age of 1 mo old (*SI Appendix*, Fig. S1*E*). In addition, male and female mice showed similar mABR thresholds (*SI Appendix*, Fig. S1*F*).

Next, we evaluated hearing and auditory transduction in hybrid *Piezo2*-cKO mice. Unless otherwise stated, their littermates were used as controls (~age 1 mo). To check whether PIEZO2 participates in ultrasonic hearing, we compared mABR of inner-ear targeted *Pax2*^{Cre};*Piezo2*$^{f/f}$ mice (18, 30) and cochlea targeted *Piezo2*-cKO mice by crossing the *Piezo2*$^{f/f}$ mice with *Atoh1*^{Cre} mice (31). The control mouse showed notable mABR signals at 32 to 80 kHz (Fig. 1*B*), while the *Pax2*^{Cre};*Piezo2*$^{f/f}$ cKO mouse showed decreased response at frequencies >32 kHz (Fig. 1*D*). This difference is clearly seen when comparing their ABR responses taken together (Fig. 1*E*). The summarized mABR recordings revealed that two types of *Piezo2*-cKO mice both had significantly reduced specific sensitivity to ultrasonic hearing (16 to 80 kHz) but not to low-frequency hearing (4 to 12 kHz) (Fig. 1*F*). Thus, these data provide convincing evidence that PIEZO2 is required for ultrasonic hearing.

In addition, we examined whether lack of ultrasonic hearing is due to loss of the "high-frequency" hair cells at the very basal coil of cochlea in the *Piezo2*-cKO mice. No obvious loss of hair cells was found in the cochleae of the *Pax2*^{Cre};*Piezo2*$^{f/f}$ cKO mice, which revealed preserved normal morphology of the hair cells (*SI Appendix*, Fig. S2). We further examined the organization of the inner ear of the *Pax2*^{Cre};*Piezo2*$^{f/f}$ cKO mouse by a tissue-clearing approach (32) (*Materials and Methods*). The whole structure of the inner ear was intact with hair cells remaining in normal allocation and abundance (Movies S1 and S2).

Ultrasonically Associative Freezing Behavior Is Disrupted in *Piezo2*-KO Mice. We investigated whether PIEZO2-mediated ultrasonic hearing sensitivity is required for learned behavior in mice. The hearing response of the *Piezo2*-cKO mice was examined by a fear conditioning test (Fig. 2*A*), which associates an acoustic cue to the freezing behavior in mice, after paired training of acoustic cues with electrical shocks. A 90-dB SPL ultrasonic 63-kHz stimulatory cue was chosen because the 63-kHz mABR showed a stable threshold difference between control and *Piezo2*-cKO mice (Fig.

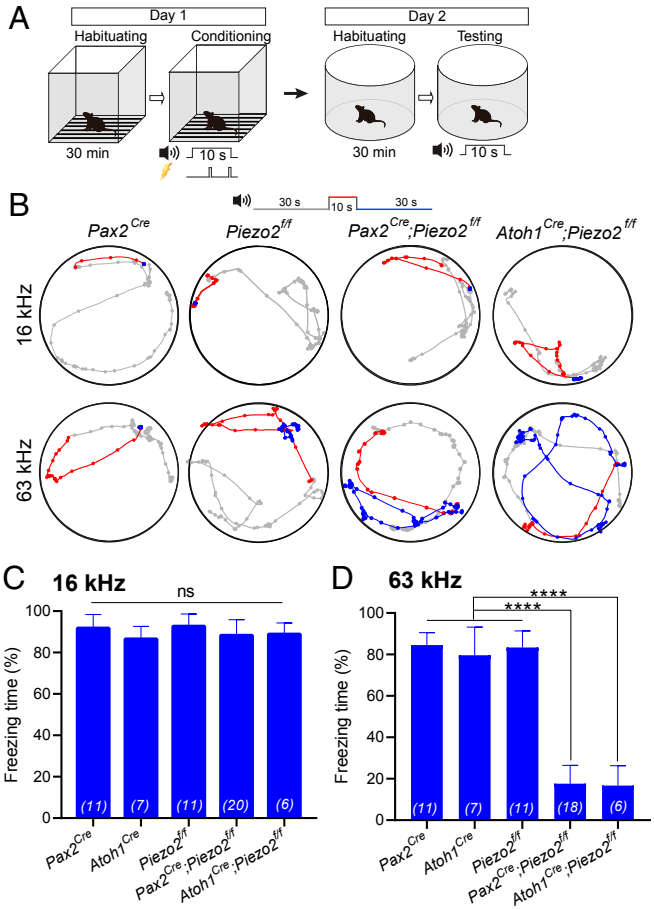

Fig. 2. Ultrasonically associative freezing behavior is disrupted in *Piezo2*-cKO mice. (*A*) Paradigm of sound-cue–associated freezing behavior. Pure-tone sound at 16 or 63 kHz played by a TDT ES1 (free field) electrostatic speaker was used as the conditional stimulation, and footshock was used as the unconditional stimulation. (*B*) Representative examples of locomotion of control mice and *Piezo2*-cKO mice before (gray, 30 s), during (red, 10 s), and after (blue, 30 s) the pure-tone sound cue at 90 dB SPL. The mice had been trained to pair either 16-kHz cue or 63-kHz cue with the footshock-induced freezing. Dots indicate the location of the mouse every 0.5 s. *Pax2*^{Cre} mice, *Atoh1*^{Cre} mice, and *Piezo2*$^{f/f}$ mice were used as controls (*C* and *D*). Freezing time in percentage is shown with 16-kHz cue (*C*) or 63-kHz cue (*D*). In *D*, experimental data from two *Pax2*^{Cre};*Piezo2*$^{f/f}$ mice were omitted because during testing, no locomotion was detected in these animals. Kruskal–Wallis test, $P = 0.225$ in *C*; one-way ANOVA, ****$P < 0.0001$ in *D*; error bars, SD. For *C* and *D*, N numbers are shown in panels. All the mice were ~1 mo old.

1*F*). Note that 63 kHz is in the range of ultrasonic frequencies of mouse social communications (1).

To exclude the possibility that disrupted ultrasonic-associative fear conditioning was due to a learning defect in *Piezo2*-cKO mice, we repeated the same experiments in control animals under identical conditions, testing freezing behavior with a 16-kHz 90-dB SPL cue. We found that harmonics appear in the 16-kHz stimulation but with lower intensities than the ABR threshold (*SI Appendix*, Fig. S3*A*). The sound intensity measured near the arena floor ranged from 75 dB SPL to 95 dB SPL (*SI Appendix*, Fig. S3*B*). This is larger than the ultrasonic hearing threshold of mice. We also examined the locomotion activity of mice with different genotypes in an open field. Control and *Piezo2*-cKO mice showed no statistical differences in locomotion distance covered in 5 min (*SI Appendix*, Fig. S3*C*).

Comparison of freezing behavior to the 90-dB 16-kHz cue for the control *Pax2*^{Cre} mice and *Piezo2*$^{f/f}$ mice with the *Pax2*^{Cre};*Piezo2*$^{f/f}$

and *Atoh1*^{Cre};*Piezo2*$^{f/f}$ cKO mice showed that all genotypes retained their low-frequency–associative freezing behavior (Fig. 2*B*). This is illustrated by the freezing time percentage (Fig. 2*C*), indicating that these mice possess low-frequency hearing and acoustically associative learning. In contrast, when exposed to the 63-kHz cue, the *Pax2*^{Cre};*Piezo2*$^{f/f}$ and *Atoh1*^{Cre};*Piezo2*$^{f/f}$ cKO mice showed disrupted freezing behavior (Fig. 2 *B* and *D*). We observed that ultrasonically conditioned learned behavior was preserved in the control mice (Fig. 2*D*). These data demonstrate that PIEZO2 is required for mice to behaviorally respond to ultrasound.

Expression of PIEZO2 in Cochlear Hair Cells. Next, we examined the expression of PIEZO2 in the cochleae. First, the *Piezo2-GFP-IRES-Cre* mice that carry a Cre cassette with the endogenous *Piezo2* (26) were crossed with the *H2B-mCherry* mice that have Cre-inducible mCherry expression (33). As previously reported (18), the mCherry expression was observed in most OHCs and some inner hair cells (IHCs) in 1-mo-old mice (*SI Appendix*, Fig. S4 *A–D*). This indicates that the *Piezo2* promoter is transcriptionally active in cochlear hair cells. Due to lack of suitable PIEZO2 antibody, we used GFP antibody to locate PIEZO2 expression in the *Piezo2-GFP-IRES-Cre* mice that is comprised of a GFP gene fused with *Piezo2*. As reported earlier (18), the PIEZO2 immunostaining signal was mainly detected at the apical surface of cochlear OHCs by the GFP antibody at P5 (Fig. 3*A*). However, this signal was faint and difficult to detect at more mature ages (~3 to 4 wk old). Thus, we applied an RNAscope protocol (34) to check the expression of *Piezo2* transcript in control and *Pax2*^{Cre};*Piezo2*$^{f/f}$ mice at P21. Within the cross-section of the organ of Corti, the *Piezo2* transcript was observed in the control *Piezo2*$^{f/f}$ hair cells though at relatively low levels, while the transcript was more significantly reduced in *Pax2*^{Cre};*Piezo2*$^{f/f}$ hair cells (Fig. 3 *B* and *C*). Control staining in either the inner ears or the dorsal root ganglia was performed to validate the effectiveness of the optimized RNAscope procedure (*SI Appendix*, Fig. S4 *E* and *F*). These data indicate that PIEZO2 is in fact expressed in the cochlear hair cells of adult mice.

Mice Lack Ultrasonic Hearing When *Piezo2* Was Deleted in OHCs. We investigated which type of hair cell supports PIEZO2's role for ultrasonic hearing by examining the ultrasound-associative freezing behavior in mice when deleting *Piezo2* in OHCs or IHCs. *Prestin*^{CreER} mice (35) were introduced to generate OHC-specific *Piezo2*-cKO mice because *Prestin* is only expressed in OHCs (36). *vGlut3*^{CreER};*Piezo2*$^{f/f}$ mice were used to check PIEZO2's role in IHCs (37). To validate the specificity of hair-cell expression, *Prestin*^{CreER};*H2B-mCherry* mice and the *vGlut3*^{CreER};*H2B-mCherry* mice were injected with tamoxifen at P8 to P10, a time with peaked expression of *Prestin* and *vGlut3*. Later, these mice were examined for mCherry expression at 1 to 2 mo old (*SI Appendix*, Fig. S5*A*). In *Prestin*^{CreER};*H2B-mCherry* mice, only the OHCs showed high efficiency mCherry expression (*SI Appendix*, Fig. S5*B*). By comparison, mCherry was widely expressed in IHCs of the *vGlut3*^{CreER};*H2B-mCherry* mice (*SI Appendix*, Fig. S5*C*).

Using the same injection procedure (Fig. 4*A*), induced *Prestin*^{CreER};*Piezo2*$^{f/f}$ cKO mice at 1 mo old showed freezing behavior when exposed to low-frequency stimulation but not to the ultrasonic cue (Fig. 4 *B* and *C*). This indicates a necessary

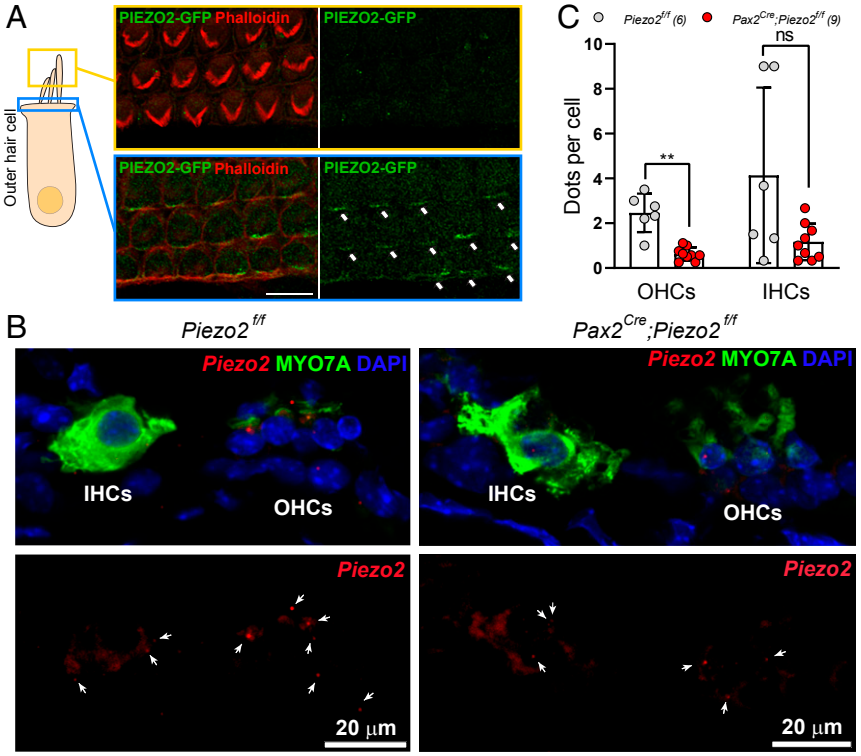

Fig. 3. Expression of Piezo2 in cochlear hair cells. (*A*) Schematic showing hair-bundle layer (yellow) and cuticular plate (blue) of an outer hair cell. Piezo2 signal (green) was detectable at cuticular plate (*Lower* in blue frame, white arrows) but not in hair bundles (*Upper* in yellow frame), as stained by GFP antibody (green) in P5 *Piezo2-GFP* mice. Hair bundle was stained by Phalloidin (red). (Scale bar, 20 μm.) (*B*) Cross-sections of organ of Corti of a *Piezo2*$^{f/f}$ mouse and a *Pax2*^{Cre};*Piezo2*$^{f/f}$ mouse at P21 showing fluorescent signals of RNAscope probe targeting *Piezo2* (red dots, indicated by arrows). Some dots were out of focus and not well visualized. Hair cells and nuclei were stained with MYO7A antibody (green) and DAPI (blue), respectively. (Scale bars, 20 μm.) (*C*) Quantification of *Piezo2* dots in cochlear hair cells from data similar to *B*. Cochlear sections were collected from P21 mice for each genotype. Note that multiple hair cells were superimposed. Numbers of transcript dots were counted per section, and numbers of hair cells were counted based on the MYO7A and DAPI signals. Unpaired *t* test with Welch's correction, OHCs, $^{**}P = 0.0026$; IHCs, $P = 0.1233$. Error bars, SD. N numbers of sections are shown in panels.

requirement of OHCs for ultrasonic hearing. On the contrary, the *vGlut3*^{CreER};*Piezo2*$^{f/f}$ mice did not show any deficit of ultrasound or low-frequency sound-associative freezing (Fig. 4 *D* and *E*), excluding a possible role of IHCs in PIEZO2-mediated function in ultrasound detection. These data confirm that expression of PIEZO2 in cochlear OHCs is required for ultrasonic hearing.

Hair-Bundle Mechanotransduction Is Required for Ultrasonic Transduction. The OHCs are capable of augmenting cochlear mechanics that enhance hearing sensitivity and frequency selectivity (38, 39). This is supported by electromotility (eM), a function that changes somatic cell shape (cellular length) with membrane potential variations in OHCs (38, 39). Thus, we sought to investigate the OHC eM in *Piezo2*-cKO mice by examining nonlinear capacitance (NLC) (40). In response to electrical stimuli, no obvious eM deficiency was found in *Pax2*^{Cre};*Piezo2*$^{f/f}$ OHCs (*SI Appendix*, Fig. S6), which is in line with previous measurements (18).

Next, we questioned whether hair-bundle mechanotransduction participates in ultrasonic transduction. It has been reported that TMC1 is the putative auditory transduction channel in hair cells, and CDH23 is one of the two tip-link components (41, 42). Thus, we used the *TMC1*-KO mice (43) and the CDH23-null *v2j* mice (44) to investigate their ultrasonic transduction. As shown by mABR recordings at 1 mo old, the two mice mutants had complete loss of hearing, which ranged from low to ultrasonic frequencies (*SI Appendix*, Fig. S7*A*). This is likely the result of abnormal hair bundles (43, 44) and loss of the hair cells (*SI Appendix*, Fig. S7 *B* and *C*). These results suggest that neither audiometry nor behavioral

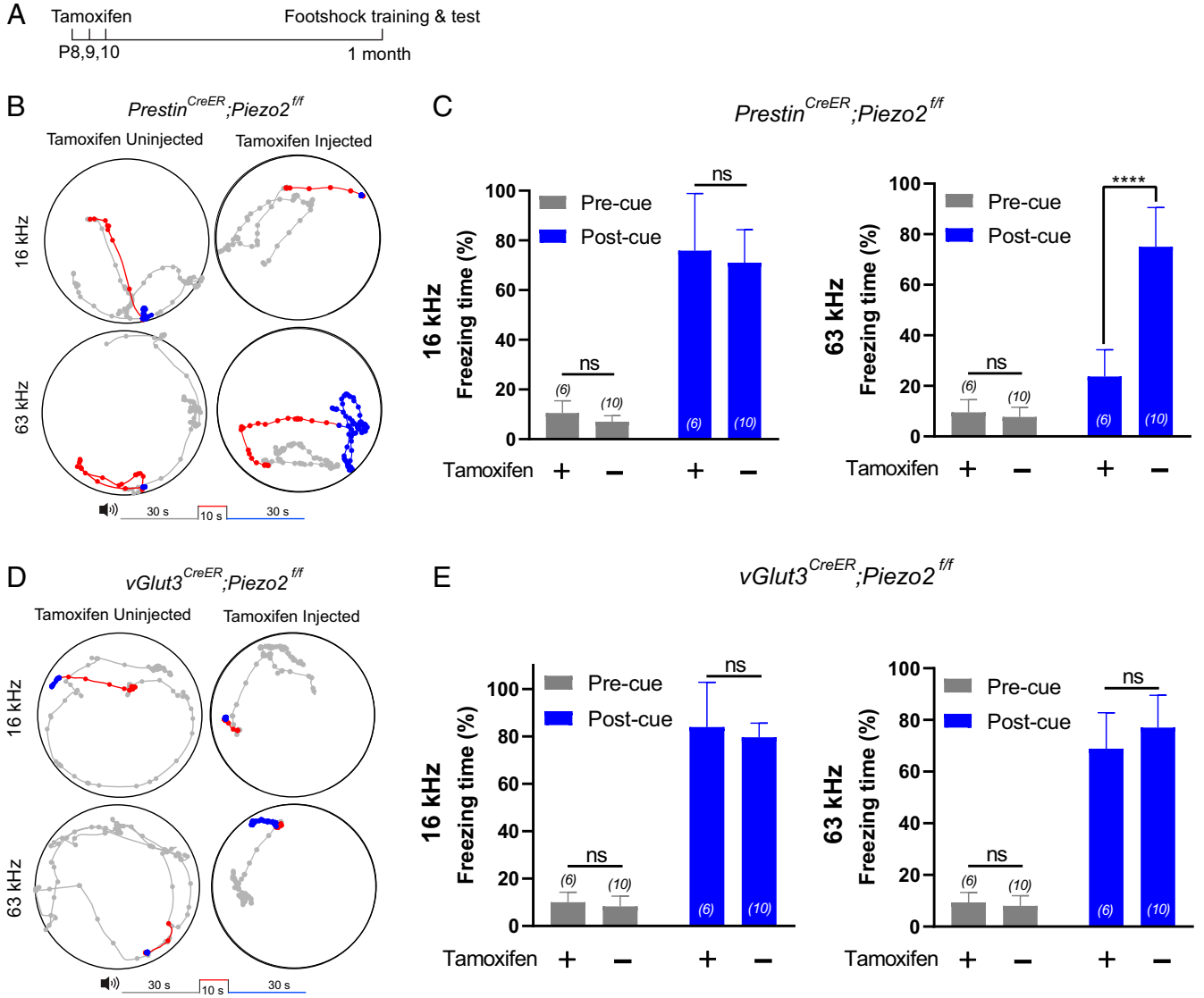

Fig. 4. Mice lack ultrasonic hearing when *Piezo2* was deleted in OHCs. (*A*) Schedule of tamoxifen injection and behavior test. (*B*) Representative example of locomotion of *Prestin*^{CreER};*Piezo2*$^{f/f}$ mice with or without tamoxifen injection. Different colors represent the locomotion before (gray), during (red), and after (blue) the 16-kHz or 63-kHz sound cue. Dots indicate the location of the mouse every 0.5 s. (*C*) Freezing time (in percentage) of the *Prestin*^{CreER};*Piezo2*$^{f/f}$ mice trained and tested with 16-kHz cue (*Left*) or 63-kHz (*Right*) cue. The comparison was performed between the tamoxifen uninjected group and the tamoxifen injected group. Sixteen kHz, precue, unpaired *t* test, $P = 0.202$; postcue, Mann–Whitney *U* test, $P = 0.513$; 63 kHz, precue, Mann–Whitney *U* test, $P = 0.4468$; postcue, unpaired *t* test, $^{****}P < 0.0001$. (*D*) Representative example of locomotion of *vGlut3*^{CreER};*Piezo2*$^{f/f}$ mice with or without tamoxifen injection. Other conditions are the same with *B*. (*E*) Freezing time of the *vGlut3*^{CreER};*Piezo2*$^{f/f}$ mice trained and tested with 16-kHz cue (*Left*) or 63-kHz (*Right*) cue. The comparison was performed between the tamoxifen uninjected group and the tamoxifen injected group. Sixteen kHz, precue, Mann–Whitney *U* test, $P = 0.3217$, postcue, unpaired *t* test, $P = 0.492$; 63 kHz, precue, Mann–Whitney *U* test, $P = 0.2052$, postcue, unpaired *t* test, $P = 0.203$. For *C* and *E*, data are presented as mean ± SD; and N numbers are shown in panels.

measures are proper probes for assessing the contribution of hair-bundle mechanotransduction. A more appropriate approach would be to use techniques targeting fine resolution of murine cellular structure and function.

To develop direct monitoring capability of ultrasonic transduction in cochlear hair cells, we customized an ex vivo ultrasonic stimulation stage. It can deliver ultrasonic vibration of 80 kHz—a frequency within the range of the physiological hearing of mice (*Materials and Methods* and *SI Appendix*, Fig. S8 *A–C*). This ultrasonic stimulation mimics the mechanical vibration in the cochlea driven by incoming ultrasound. One obstacle to this experiment was obtaining an intact organ of Corti from mice after hearing onset because the cochlea has been embedded into the bony capsule of the inner ear. Instead, we introduced a hemicochlear preparation (45, 46) that preserves most of the elements of the cochlea and is also accessible to microscopic observation (Fig. 5*A*). Because patch-clamp recording of hair cells is routinely destroyed by direct ultrasonic stimulation, we used Ca^{2+} imaging for monitoring ultrasonically evoked activity (Fig. 5*B*).

The hemicochlear preparation was loaded with Fluo-8 AM, a sensitive Ca^{2+} dye. The OHCs were the major cells with Ca^{2+} dye uptake (Fig. 5*C*). Ultrasonic stimulation elicited Ca^{2+} waves in the OHCs of wild-type (WT) hemicochleae despite apical or middle positioning in the cochlear coil. This effect could be blocked when perfusing cells with 0.1 mM Ca^{2+} solution (*SI Appendix*, Fig. S8 *D* and *E*), which suggests that the OHCs are ultrasonically responsive. After ultrasonic stimulation, the Fluo-8–loaded OHCs showed an evoked Ca^{2+} wave when ATP (100 μM) was applied (*SI Appendix*, Fig. S8 *D* and *E*). This indicates that the OHCs were healthy after ultrasonic stimulation and that the Ca^{2+} response was not saturated.

We evaluated the role of PIEZO2 and TMC1 in ultrasonic transduction by hemicochlear Ca^{2+} imaging. Ultrasonic stimulation was capable of eliciting Ca^{2+} responses in OHCs of the control *Piezo2*$^{f/f}$ mice. However, when *Piezo2* was genetically removed from the OHC, Ca^{2+} response was significantly diminished (Fig. 5 *D* and *E* and Movies S3 and S4). Although OHCs were widely lost in *Tmc1*-KO mice from 3-wk-old litters (*SI Appendix*, Fig. S7*B*) (43), we could readily identify apical OHCs with clear soma shapes illuminated by Fluo-8 for Ca^{2+} imaging. The ultrasonic Ca^{2+} response was significantly reduced in the *Tmc1*-KO OHCs or in WT OHCs blocked by the mechanotransduction channel-blocker dihydrostreptomycin (DHS, 100 μM) (Fig. 5 *F* and *G*). This implies that hair-bundle mechanotransduction is a requirement in ultrasonic transduction.

To investigate the response evoked by low-frequency stimulation, we used fluid jet, a stimulation which directly deflects the hair bundle to induce the mechanotransduction channel-mediated Ca^{2+} response in *Tmc1*-KO or *Pax2*^{Cre};*Piezo2*$^{f/f}$ OHCs. Similar to ultrasonic frequencies, there is no fluid-jet–evoked Ca^{2+} response in *Tmc1*-KO OHCs. In contrast, the fluid-jet–induced Ca^{2+} response was maintained in *Pax2*^{Cre};*Piezo2*$^{f/f}$ OHCs and WT OHCs (Fig. 5 *H* and *I*). These ex vivo results showed that PIEZO2 is required for the OHC Ca^{2+} response stimulated by ultrasonic frequencies but not for those stimulated by low frequencies. We further tested whether PIEZO2 and/or TMC1 could establish the ultrasonic transduction in exogenous expression systems. Although the human embryonic kidney 293T (HEK293T) cells expressing PIEZO2 were mechanosensitive (*SI Appendix*, Fig. S9 *A* and *B*), we did not observe any response in the HEK293T cells expressing PIEZO2 or PIEZO2 plus TMC1 when using the same 80-kHz ultrasonic stimulation applied for hemicochlear imaging (*SI Appendix*, Fig. S9 *C* and *D*). These results show that PIEZO2 may coordinate with the hair-bundle mechanotransduction machinery to effectuate ultrasonic transduction.

Discussion

We have shown that multiple lines of evidence suggest that PIEZO2 is essential for mice hearing ultrasonic frequencies within the range necessary for social communication. Furthermore, ultrasonic transduction is mainly conducted by OHCs, which coordinates hair-bundle mechanotransduction. Small mammals, such as mice, emit strong ultrasonic vocalization for social communication while overriding ambient noise, or masking sound emissions, which escape potential detection by predators. This paper posits a putative molecular and cellular mechanism underlying ultrasonic hearing and transduction, which, heretofore, has not been established.

It has been shown that with low-level *Piezo1* expression, PIEZO1-mediated mechanically activated current can be detected in HEK293T-derived cell lines (47). PIEZO2's structure and mechanosensitivity properties likely support its role for OHCs in ultrasonic transduction. Previous evidence has shown that in mice neonates, PIEZO2 is expressed in cochlear hair cells (18). Our findings suggest that PIEZO2 expression in OHCs continues to at least weeks 3 to 4 (Fig. 3 *B* and *C*). *Piezo2* expression shown by RNAscope assays is low, which may not reflect the quantity of PIEZO2 in OHCs.

PIEZO2 is a mechanosensitive channel that homotrimerizes to form a gigantic (~0.9 MDa) three-bladed propeller-like structure comprising 114 transmembrane (TM) domains (38 TM per protomer), making it a unique membrane protein with the largest number of TMs (16). There are three strikingly unusual nonplanar TM blades that are curved into a nano-bowl shape of 28-nm diameter and 10-nm depth, which might deform the residing membrane to produce a midplane nano-bowl surface area of 700 nm^2 and a projected in-plane area of 450 nm^2. On the basis of the unique nano-bowl shape of the Piezo channel-membrane system, flattening the nonplanar TM blades may produce a maximal change of the projection area of ~250 nm^2, generating energy to gate the channel (16). The curved configuration of the Piezo channels (PIEZO1 and PIEZO2) may further deform the membrane shape outside of the perimeter of the channel into a large, curved "membrane footprint" (48), which could further amplify the mechanosensitivity of the Piezo channel. Such "membrane-dome" (49) and "membrane footprint" (48) mechanisms have been proposed to account for the exquisite mechanosensitivity of PIEZO channels in response to various mechanical stimulation including poking and stretch forces. This would be an essential function of PIEZO1's response to nonphysiological ultrasonic stimulation (0.5 MHz) (50).

We speculate that one of PIEZO2's roles is to coordinate with hair-bundle mechanotransduction machinery to achieve ultrasonic transduction. Removal of either PIEZO2 or TMC1 abolished ultrasonic transduction (80 kHz) in cochlear hair cells (Fig. 5 *D–G*). This suggests that both PIEZO2 and hair-bundle mechanotransduction are required for ultrasonic transduction and explains why HEK293T cells expressing PIEZO2 fail to show ultrasonic response (*SI Appendix*, Fig. S8). PIEZO2 may be located at the apical surface of the OHCs, more specifically at the reticular lamina, where the stereocilia roots are least influenced by the membrane low-pass filtering. It cannot be excluded that PIEZO2 detects ultrasonic waves via adhesive junctions between OHCs and supporting cells (18) at the reticular lamina. In coordination with the vibration at the reticular lamina, which shakes the stereocilia from their roots, the hair-bundle mechanotransduction channels are activated reciprocally. Thus, it is possible that PIEZO2 itself may function only to detect ultrasonic waves rather than transducing them. We are intrigued with the idea that these data collected during auditory transduction may reflect functional consolidation of the two molecularly distinct mechanotransduction channels.

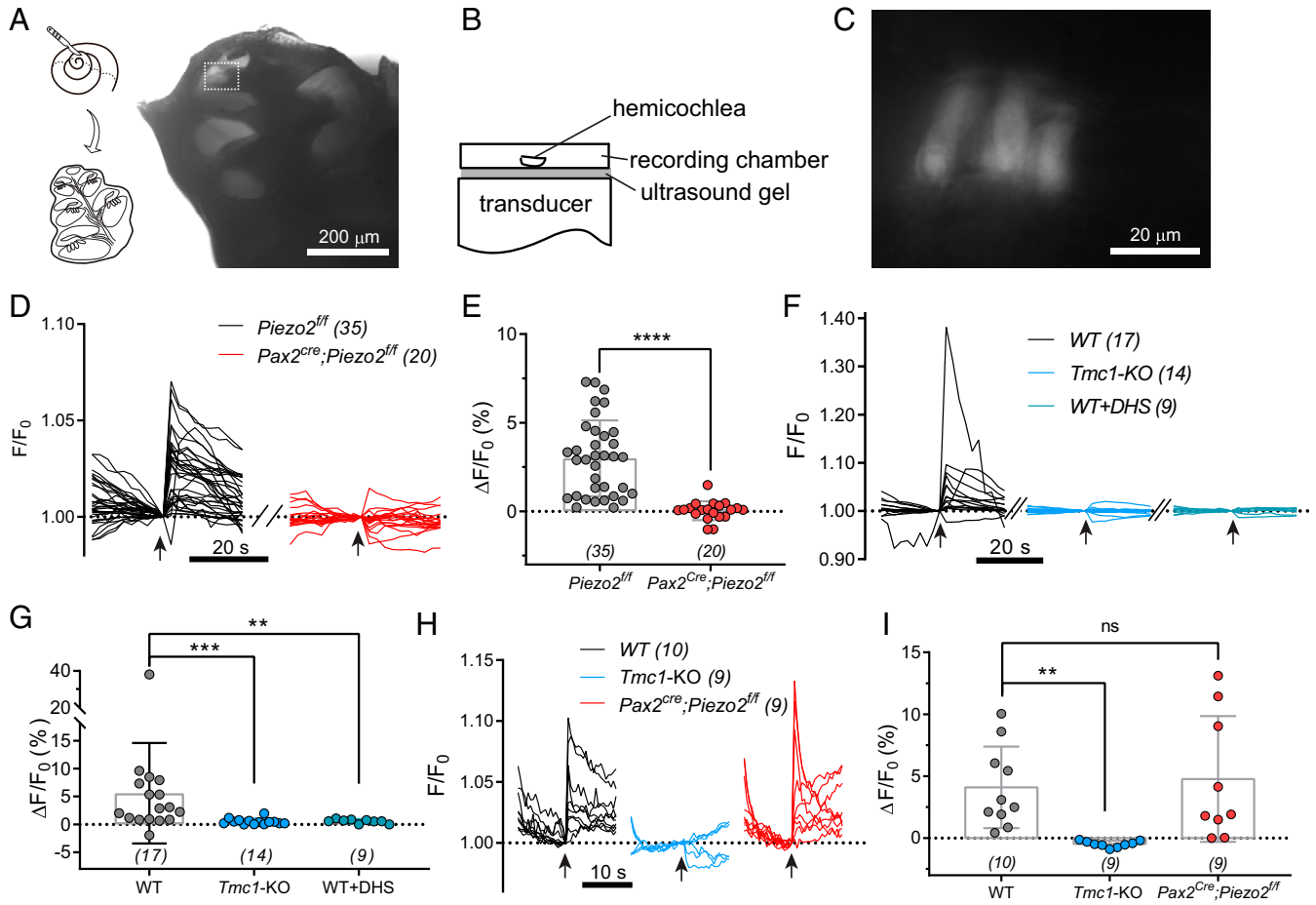

Fig. 5. Hair-bundle mechanotransduction is required for ultrasonic hearing. (*A*, *Left*) Schematic showing preparation of hemicochlea. (*Right*) A photograph of hemicochlea with transmission-light illumination. (Scale bar, 200 μm.) (*B*) Setup for ultrasonic transducer stimulated hemicochlea. An 80-kHz transducer was fixed underneath the recording dish with ultrasound gel in between. (*C*) A fluorescent image showing Fluo-8 AM–loaded OHCs, magnified from the apical part (white-dashed frame) of the hemicochlea in *A*. (Scale Bar, 20 μm.) (*D*) Ultrasonic stimulation evoked Ca^{2+} responses of OHCs in hemicochlea preparations from control *Piezo2*$^{f/f}$ mice (black) and *Pax2*^{Cre};*Piezo2*$^{f/f}$ cKO mice (red). Arrows indicate the onset of ultrasonic stimulation. The images were collected at 2-s intervals (reference Movies S3 and S4). (*E*) Quantification of the peak Ca^{2+} responses of OHCs calculated from recordings in *D*. Unpaired *t* test with Welch's correction, $^{****}P < 0.0001$. (*F*) Ultrasonic stimulation evoked Ca^{2+} responses of OHCs from WT hemicochleae, *Tmc1*-KO hemicochleae, and WT hemicochleae treated with 100 μM DHS. (*G*) Quantification of the peak Ca^{2+} responses of OHCs calculated from recordings in *F*. Kruskal–Wallis test was performed for group comparison, WT hemicochleae versus *Tmc1*-KO hemicochleae, $^{***}P = 0.0001$; WT hemicochleae versus WT hemicochleae treated with 100 μM DHS, $^{**}P = 0.0069$. (*H*) Low-frequency fluid-jet–evoked Ca^{2+} responses of OHCs in hemicochlea preparations from WT, *Tmc1*-KO, and *Pax2*^{Cre};*Piezo2*$^{f/f}$ cKO mice. (*I*) Quantification of the peak of OHCs in hemicochlea preparations from WT, *Tmc1*-KO, and *Pax2*^{Cre};*Piezo2*$^{f/f}$ cKO mice from similar recordings in *H*. Brown–Forsythe ANOVA test, WT hemicochleae versus *Tmc1*-KO hemicochleae, $^{**}P = 0.0032$; WT hemicochleae versus *Pax2*^{Cre};*Piezo2*$^{f/f}$ cKO hemicochleae, $P = 0.9215$. For *E*, *G*, and *I*, data are presented as mean ± SD, and N numbers are shown in panels. In this figure, all the mice were tested at ~1 mo old.

PIEZO2-mediated ultrasonic sensitivity in OHCs evolves over time. As Wu et al. proposed (18), the mechanosensitivity mediated by PIEZO2 and related Ca^{2+} modulation may support normal development of hair cells. However, in the first neonatal week, hair-bundle structure and function are still under development and are immature. This delay in maturation prevents the OHCs from accurately distinguishing the two PIEZO2 and mechanotransduction channels in their physiological functions. This sets into motion a process whereby the cell's mechanotransduction machinery becomes asynchronous. This can result in the disruption of stereociliary mechanotransduction that subsequently unmasks PIEZO2-mediated mechanotransduction (18, 20).

On the other hand, the PIEZO2-mediated mechanotransduction may provide backup support for hair-bundle mechanotransduction (18), existing in both OHCs and IHCs. In mice at neonatal stage, *Piezo2* expression is found in both types of hair cells. After the onset of hearing, the two mechanotransduction channels establish their separate physiological specializations, respectively—hair-bundle–based machinery itself is enough for sonic transduction, while at ultrasonic range, PIEZO2 orchestrates hair-bundle mechanotransduction machinery supporting auditory transduction.

Interestingly, the cochlear OHCs, not the IHCs, are the effectors enabling PIEZO2 to sense ultrasound emissions (Fig. 4). This is the mechanism by which the animal gains extended spectral sensitivity from 16 kHz toward ultrasonic frequencies (Fig. 1*F*). Another OHC-specific protein is Prestin, a moiety that enhances cochlear mechanics and hearing sensitivity by providing OHCs somatic eM, which is not affected by PIEZO2 ablation. With PIEZO2, it is possible that the OHCs use a mechanism like ciliary motility to transfer ultrasonic vibration to the IHCs through the relative motion between the tectorial membrane and the reticular lamina. However, this putative mechanism needs further empirical evidence. The IHC may simply output the encoded ultrasound information from the organ of Corti. This is implied by evidence that the induced *vGlut3*^{CreER};*Piezo2*$^{f/f}$ mice have normal ultrasonic freezing (Fig. 4 *D* and *E*).

A similar examination of *Piezo2*-null mice with ABR measurement was previously reported by Wu et al. (18) but in the lower frequency range. The authors suggest that mild differences (<10 dB) in ABR thresholds were observed in 12 to 28 kHz between *Piezo2*-cKO and $Pax2^{Cre}$ mice, which are similar with our results (Fig. 1*F*). However, the observation that *Piezo2*-cKO and $Pax2^{Cre}$ mice have similar ABR thresholds at 32 kHz seems at variance with our findings. Additionally, in our study, the control $Pax2^{Cre}$ mice had similar mABR thresholds with the B6 mice (Fig. 1 *C* and *D*), which is slightly different from their observation that the 2-mo $Pax2^{Cre}$ mice showed higher ABR thresholds (18).

Several factors may contribute to these differences. First, the two studies used different ABR electrode configurations. Using an electrode gently implanted in the skull in apposition to the brain, the mABR configuration was adapted to achieve higher stability and sensitivity. This is especially relevant for ABR signaling in the ultrasonic hearing range. Second, for ABR testing we used less developmentally mature 1-mo-old mice compared to the other study's 2-mo-old cohort. Hearing sensitivity at different ages may vary slightly. Third, different genetic backgrounds for generating hybrid mice may result in shifts in their physiological functionality. Our data show that ultrasonic hearing is established, at minimum, from P21. Thus, the majority of our recordings were collected from 1-mo-old mice with their littermates used as controls. This was done to avoid the possibility of progressive deterioration that could result in erroneous data production.

In summary, we have discovered that PIEZO2 in OHCs plays an indispensable role in ultrasonic high-frequency hearing, suggesting an alternative auditory transduction mechanism for encoding frequencies in mammals. Given that both ultrasonic hearing and low-frequency hearing are conducted via cochlear OHCs but may be based on different mechanisms, it is of interest to investigate the response patterns to ultrasonic frequencies in cochlea, that is, whether such patterns follow the place-code principle of apical OHCs for low-frequency hearing, and very basal OHCs for ultrahigh-frequency hearing. It would be intriguing to study PIEZO2's role in ultrasonic hearing from other species, for example, bats and whales. Furthermore, our study lays the foundation for addressing whether ultrasonic hearing and low-frequency hearing use distinct neural circuits and processing principles in brain regions along the ascending auditory pathways.

Materials and Methods

Mouse Strains and Animal Care. In this study, $Cdh23^{v\text{-}2j}$ mice (stock no. 002552, named *Cdh23*-null in this study), B6.129-$Tmc1^{tm1.1Ajg}$/J mice (stock no. 019146, named *TMC1*-KO in this study), and *Rosa26 LSL H2B mCherry* mice (stock no. 023139, named *H2B-mCherry* in this study) were from the Jackson Laboratory (Bar Harbor, ME); *Pax2-Cre* mouse line (named $Pax2^{Cre}$ in this study) was generated by Dr. Andrew Groves at Baylor College of Medicine (30) and *Atoh1-Cre* mice (named $Atoh1^{Cre}$ in this study) were kindly from Dr. Lin Gan in the Medical College of Georgia at Augusta University (31); $Piezo2^{loxP/loxP}$ (named $Piezo2^{f/f}$ in this study) and *Piezo2-GFP-IRES-Cre* mice were gifts from Dr. Ardem Patapoutian at the Scripps Research Institute (26); Prestin-CreER^{T2} ($Prestin^{CreER}$ in this study) mouse line was a gift from Dr. Jian Zuo in School of Medicine at Creighton University (35); and *vGlut3-P2A-iCreER* knockin mouse strain was generated as described (37) and here named as $vGlut3^{CreER}$ mouse. All the cKO mice were crossed in mixed genetic background, and their littermates were selected as controls for each experiment. No obvious difference in body size and weight (wt) was noticed in the littermates. Tamoxifen (Sigma, 20mg/mL in corn oil) was injected intraperitoneally (ip) into the mice with *CreER* background at P8 with a dose of 3mg/40g (tamoxifen/body wt). The mice were injected once a day for 3 d (37). The experimental procedures on mice were approved by the Institutional Animal Care and Use Committee of Tsinghua University.

mABR. Mice of either sex were anesthetized (ip) with 0.4% pentobarbital sodium in saline (0.2 mL/10 g, volume[vol]/body wt). Body temperature was maintained at 37 °C by a heating pad during the entire experiment. After the skin on the vertex was removed, the skull was exposed and a stainless-steel screw was attached (M1.4 × 2.5) but did not puncture the dura. The recording electrode was connected to the screw by a silver wire with a diameter of 0.1 mm. Other operations were similar to regular ABR procedure. The reference and ground electrodes were inserted subcutaneously at the pinna and the groin, respectively. The mice harboring a bone attachment in Type-A implantation (an electrode implanted at −7 mm AP, 0 mm ML referred to the Bregma point) best exhibited the ultrasonic responses (*SI Appendix*, Fig. S1), which were used in this study. The ABR data were collected with ∼200-kHz sampling rate by an RZ6 workstation controlled by a BioSig software (Tucker-Davis Technologies). Clicks and 4 to 16 kHz pure-tone bursts were generated by a TDT MF1 closed-field magnetic speaker while a TDT EC1 (Coupler Model) electrostatic speaker was used for generating high frequencies (32 to 80 kHz). For the sound stimulation, 0.1-ms duration of click stimulus and 5-ms duration with 0.5-ms rise-fall time of tone bursts were delivered at 21 Hz, with intensities from 90 to 10 dB SPL in 10-dB steps. Upon each acoustic stimulation with defined frequency and intensity level, the responses were sampled 512 times repeatedly and then averaged. The lowest stimulus sound level at which a repeatable wave 1 could be identified was defined as the threshold as previously reported (51).

Acoustic-Cue–Associated Freezing Behavior. Male mice were used. Mouse locomotion in an operant box (cubic, 30 × 30 × 30 cm) or an activity box (cylindrical, diameter of 35 cm and height of 30 cm) was monitored by an infrared camera with an infrared light as the light source, which was performed in a soundproof chamber (Shino Acoustic Equipment Co., Ltd.). Each mouse was allowed to freely explore the operant box for 30 min before the sound-associated footshock training. During the training, an acoustic cue of 10 s containing 50 ms pure tone (16 or 63 kHz) at 50-ms interval was played, and electrical shocks of 1 s at current magnitude of 0.6 mA were given to the mouse at the 5th s and 10th s. In the operant box, the electrical shocks were delivered by the metal grid floor powered by an electrical stimulator (YC-2, Chengdu Instrument Inc.), and the acoustic cues were given by a free-field electrostatic speaker ES1 placed 15 cm above the floor and powered by an RZ6 workstation and a BioSig software (Tucker-Davis Technologies). The cue was given every 3 min and repeated for 10 times before the trained mouse was put back to the home cage. After 24 h, the trained mouse was transferred in an activity box to test freezing behavior. In the activity box, the same ES1 speaker was placed 15 cm above the chamber floor to generate the 16 or 63 kHz acoustic cues of 10 s duration (identical to the training cues), and cues were given at least five times during the test procedure. As calibrated, the sound intensity on the arena floor was from 70 to 90 dB SPL, which is in the range of mouse hearing threshold (*SI Appendix*, Fig. S3).

Open-Field Test. Male mice at 1-mo age were used. The mice were put in a cylindrical box with a diameter of 35 cm and height of 30 cm that was a new place to them. Locomotion was recorded with an infrared camera and illuminated with an infrared light-emitting diode (LED). The distance a mouse traveled in the first 5 min was calculated with MATLAB 2014b (MathWorks).

Immunostaining. The mice were selected for immunostaining at indicated ages. After anesthesia with Avertin (30 mg/mL in saline, 0.12 to 0.15 mL/10g for mice), the mouse was perfused with ice-cold phosphate buffered saline (PBS) and euthanized by decapitation. The inner ears were dissected from the temporal bone. Then, the inner ears were fixed by fresh 4% paraformaldehyde (PFA) (DF0135, Leagene) in PBS for 12 to 24 h at 4 °C. After fixation, the inner ears were washed with PBS three times (10 min for each time) and then were treated in 120 mM EDTA decalcifying solution (pH 7.5) for 24 h at room temperature (RT, 20 to 25 °C) followed by PBS washing. The cochlear coils were finely dissected from the inner ears in PBS and blocked in 1% PBST (PBS + 1% Triton X-100 [T8787, Sigma-Aldrich]) solution with 5% bovine serum albumin (BSA) (A3059, Sigma-Aldrich) at RT for 1 h. The cochlear tissues were then incubated in 0.1% PBST 5% BSA solution with MYO7A antibody (1:1,000, Catalog [cat.] 25-6790, Proteus Biosciences Inc.) overnight at 4 °C and washed with 0.1% PBST three times at RT. The tissues were incubated with secondary antibody (Invitrogen anti-Rabbit Alexa Fluor 647, 1:1,000, A21244; Invitrogen Alexa Fluor 488 Phalloidin, 1:1,000, Cat. A12379) and 1:1,000 DAPI in 0.1% PBST 5% BSA solution at RT for 2 to 4 h. Tissues were washed with 0.1% PBST three times and mounted by ProLong Gold Antifade Mountant (Cat. P36930, Life Technology). The photographs of fluorescent immunostaining pattern were collected by an A1 confocal microscope (A1 N-SIM, Nikon). The whole-view photographs of the cochlear tissues were stitched by Photoshop software (version 9.3.1, Bitplane, Oxford instruments). The immunostaining procedure of cochlear tissues from *Piezo2-GFP* mice was slightly changed based on the immunostaining protocol above. For fixation, the inner ears were perfused by 2% fresh PFA and incubated at RT for 30 to 45 min without shaking. For blocking, the cochlear tissues were

treated in 0.5% PBST solution with 4% BSA at RT for 2 h with slow shaking. The tissues were incubated overnight at 4 °C with the primary antibody (Rabbit anti-GFP; 1:500, Cat. A-11122, ThermoFisher Scientific) that was made in 0.5% PBST with 1% BSA and then washed with 0.1% PBST three times. Then, the cochlear tissues were incubated in the secondary antibody (Invitrogen anti-Rabbit Alexa Fluor 647, 1:1,000, Cat. A21244; Invitrogen Alexa Fluor 568 Phalloidin, 1:1,000, Cat. A12380) that was made in 0.5% PBST solution. Each incubation was shaken slowly.

Inner Ear Clarification. We used the polyethylene glycol (PEG)-associated solvent system (PEGASOS) method for inner ear clarification as previously reported (32). Mice were anesthetized by 0.4% pentobarbital sodium with an ip injection, followed by transcardiac perfusion with ice-cold 0.01 M PBS to wash out blood and then with 4% PFA. The inner ear was dissected in 4% PFA and fixed for 12 h at RT. After that, the following steps were performed in 37 °C shaker. The inner ear was immersed in 0.5M EDTA for 2 d with daily change for decalcification and ddH_2O for 2 h to wash out remaining salt. Next, the inner ear was immersed in 25% Quadrol (diluted with H_2O to a final concentration of 25% vol/vol, 122262, Sigma-Aldrich) for 2 d with daily change and 5% ammonium solution (diluted with H_2O to a final concentration of 5% vol/vol, 105432, Sigma-Aldrich) for 6 h to decolorize. Then, ammonium solution was washed out with PBS for 30 min, followed by immunostaining steps. The inner ear was first immersed in blocking solution (4% BSA [V900933, VETEC] in 0.5% PBS-Triton X-100 [T8787, Sigma-Aldrich]) for 1 d, followed by Myo7a antibody (1:800, Rabbit, 25-6790, Proteus Biosciences) in blocking solution for 2 d with daily change. Then, first antibody was washed out with 0.5% PBS-Triton X-100 for 1 d. Goat anti-Rabbit secondary antibody Alexa Fluor 488 (1:800, A11008, ThermoFisher) in blocking solution was used to incubate for 2 d with daily change, also followed by washing out with PBS for 1 d. After that, de-lipidation was performed with the inner ear immersed in 30% tert-butanol (diluted with H_2O, 360538, Sigma-Aldrich) for 4 h, 50% tert-butanol for 6 h, and 70% tert-butanol for 1 d. Then, the inner ear was immersed in tert-butanol (tB)-PEG (70% vol/vol tert-Butanol, 27% vol/vol PEG methacrylate Mn 500 [PEGMMA500] [409529, Sigma-Aldrich], and 3% wt/vol Quadrol) for 2 d with daily change for delipidation and BB-PEG (75% vol/vol benzyl benzoate [BB] [W213802, Sigma-Aldrich], 22% vol/vol PEGMMA500, and 3% wt/vol Quadrol) for 2 d with daily change for clearing. Clarified inner ear was imaged with light-sheet microscope (Zeiss, Lightsheet Z.1) using 5× objective lens.

RNAscope Detection. After anesthesia with Avertin, transcardiac perfusion was done in P21 mice with ice-cold DEPC-PBS and then with 4% PFA (dilute from 16% PFA, DF0131, Leagene) in DEPC-PBS. Then, the temporal bones were dissected and fixed in fresh 4% PFA in DEPC-PBS at 4 °C for 12 h. After the postfixation, the cochleae were decalcified by incubating at 120 mM EDTA decalcification solution at RT for 48 to 60 h. Then, the cochleae were dehydrated in 15% sucrose solution in DEPC-PBS for about 30 min at 4 °C and in 30% sucrose solution in DEPC-PBS for about 2 h until the cochleae sunk to the bottom of the tubes. After that, the cochleae were embedded in O.C.T (optimal cutting temperature) (4583, Tissue-Tek) and stored at −80 °C. The embedded tissues were sliced into 14-μm sections (CryoStarTM NX50, ThermoFisher Scientific) and stored at −20 °C no more than 8 h before RNAscope detection. The *Piezo2* transcript detection was performed according to manufacturer's instructions using RNAscope detection kit (323100, ACDBio). Optimizing the procedure was time consuming because of difficulty keeping the organ of Corti in its original shape and sticking to the glass slide after stringent treatments. This procedure was also tested by control probes (*SI Appendix*, Fig. S4*E*). The probe of *Piezo2* (439971, ACDBio) was validated by staining in dorsal root ganglion (DRG) tissue slice (*SI Appendix*, Fig. S4*F*). The sections of organ of Corti from control and *Piezo2*-cKO mice were placed on the same glass slide and subjected to identical RNAscope procedures and imaging conditions.

Hemicochlear Imaging. Mice at 1-mo age were anesthetized by isoflurane and euthanized. Then, their cochleae were dissected out in the dissection solution containing the following (in mM): 5.36 KCl, 141.7 NaCl, 1 $MgCl_2$, 0.5 $MgSO_4$, 0.1 $CaCl_2$, 10 H-Hepes, 3.4 L-Glutamine, and 10 D-Glucose (pH 7.4, Osmolarity at 290 mmol/kg). After immersion in the cutting solution containing (in mM) 145 NMDG-Cl, 0.1 $CaCl_2$, 10 H-Hepes, 3.4 L-Glutamine, and 10 D-Glucose (pH 7.4, Osmolarity at 290 mmol/kg), the cochlea was glued on a metal block with Loctite 401 and cut into two halves by a vibratome (VT1200S, Leica) with frequency index at 7, speed index at 50. The section plane was maintained in parallel to the modiolus to minimize the damage on tissue. The hemicochlea was transferred into a recording dish, glued on the bottom, and loaded with 25 μg/mL Fluo-8 AM (Invitrogen) in the recording solution. After 10-min incubation at RT in a dark box, the dye-loading solution was replaced by the dye-free recording solution containing (in mM): 144 NaCl, 0.7 Na_2PO4, 5.8 KCl, 1.3 $CaCl_2$, 0.9 $MgCl_2$, 10 H-Hepes, and 5.6 D-Glucose (pH 7.4, Osmolarity at 310 mmol/kg). An upright microscope (BX51WI, Olympus) equipped with 60× water-immersion objective (LUMPlanFL, Olympus) and an sCMOS (scientific complementary metal-oxide-semiconductor) camera (ORCA Flash 4.0, Hamamatsu) was used for calcium imaging, controlled by MicroManager 1.6 software (52) with a configuration of 4 × 4 binning, 100-ms exposure time, and 2-s sampling interval. To maintain the best performance of the hemicochlea preparations, the entire procedure from cutting to imaging was finished within 15 min to guarantee the best appearance of tissue samples. As control experiments, 0.1 mM Ca^{2+} (to keep tip-link structure) perfusion abolished the ultrasonic stimulation evoked Ca^{2+} signal, and 100 μM ATP perfusion induced strong Ca^{2+} response (~20%), in the OHCs of the hemicochleae.

Ultrasound Generation and Delivery Ex Vivo. A customized 80-kHz ultrasound transducer with a diameter of 27 mm was powered by a radio-frequency amplifier (Aigtek, ATA-4052) integrated with a high-frequency function generator (Rigol, DG1022U). The 80-kHz transducer was chosen because its size is small enough to be assembled (the lower the frequency, the larger the size), and 80 kHz is a physiological frequency for mice. For calibration, a high-sensitivity hydrophone (Precision Acoustics) was positioned directly above the vibration surface. Transducer outputs were calibrated in a tank filled with deionized, degassed water under free-field conditions. To stimulate hemicochlea, the transducer was tightly fixed at the bottom of recording dish with ultrasound gel in between. The distance between the tissue and ultrasound transducer was less than 5 mm. For the 80-kHz ultrasonic stimulation, a single pulse of 100 ms was applied, with calibrated intensities at 8.91 W/cm^2 I_{SPTA}. The ultrasound energy received by the tissue preparation was stable and homogeneous, as shown by calibrated intensities covering the whole bottom of the recording dish (*SI Appendix*, Fig. S7).

Low-Frequency Fluid-Jet Stimulation to Hemicochlea. Fluid-jet configuration was used as previously reported (53). Briefly, a 35-mm diameter circular piezoelectric ceramic was sealed in a self-designed mineral oil tanker. An electrode with 5- to 10-μm diameter tip filled with recording solution (144 NaCl, 0.7 Na_2PO_4, 5.8 KCl, 1.3 $CaCl_2$, 0.9 $MgCl_2$, 10 H-Hepes, 5.6 D-Glucose in mM, pH 7.4, Osmolarity at 310 mmol/kg) was mounted into the tanker and transmitted the pressure wave to the hair bundle of an OHC in hemicochlea samples. The circular piezoelectric ceramic was driven by a sinusoidal voltage fluctuation generated from a patch-clamp amplifier (EPC10 USB, HEKA Elektronik) and amplified at 20-fold with a custom high-voltage amplifier. The 100-ms sinusoidal stimulation was given at frequency of 2,000 Hz and amplitude of 6.5 V.

Single-Cell Ca^{2+} Imaging and Whole-Cell Electrophysiology. HEK293T cells were plated onto 8-mm round glass coverslips, which were coated with poly-D-lysine and placed in 48-well plates. A total of 400 ng of plasmids were transiently transfected into HEK293T cells using lipofectine 2000 (Life Technologies). GCaMP6 was expressed to monitor the Ca^{2+} response. After 24 h transfection, the HEK293T cells were imaged for Ca^{2+} signals by an upright microscope (BX51WI, Olympus) equipped with 60× water-immersion objective (LUMPlanFL, Olympus) and an sCMOS camera (ORCA Flash 4.0, Hamamatsu), controlled by MicroManager 1.6 software (52) with 50-ms exposure time and 1-s sampling interval. HEK293T cells were recorded using whole-cell patch clamp as previously described (54). All experiments were performed at RT (20 to 25 °C). Briefly, the coverslip with cultured cells was transferred into a recording chamber with recording solution containing the following (in mM): 144 NaCl, 0.7 NaH_2PO_4, 5.8 KCl, 1.3 $CaCl_2$, 0.9 $MgCl_2$, 5.6 glucose, and 10 H-Hepes (pH 7.4). The cells were imaged under an upright microscope (BX51WI, Olympus) with a 60× water-immersion objective and an sCMOS camera (ORCA Flash4.0, Hamamatsu) controlled by MicroManager 1.6 software (52). Patch pipettes were made from borosilicate glass capillaries (BF150-117 -10, Sutter Instrument Co.) with a pipette puller (P-2000, Sutter) and polished on a microforge (MF-830, Narishige) to resistances of 4 to 6 MΩ. Intracellular solution contained the following (in mM): 140 KCl, 1 $MgCl_2$, 0.1 EGTA, 2 Mg-ATP, 0.3 Na-GTP, and 10 H-Hepes, pH 7.2. The cells were recorded with a patch-clamp amplifier with a holding potential of −70 mV (EPC 10 USB and Patchmaster software, HEKA Elektronik). The liquid junction potential is not corrected in the data shown. As measured, the pipette with CsCl intracellular solution had a value of +4 mV in regular recording solution.

Mechanical stimulation utilized a fire-polished glass pipette (tip diameter 3 to 4 mm) positioned at an angel of 80 relative to the cell being recorded as

described (54). The probe was displaced by a piezoelectric actuator (P-601.1SL, Physik Instrumente) and driven by a piezoelectric crystal microstage (E625 LVPZT Controller/Amplifier, Physik Instrumente). The probe velocity was 1 μm/ms during the upward and downward movement, and the stimulus was kept constant for 100 ms. A series of mechanical steps in 1-μm increments was applied every 5 to 10 s.

NLC Recording. Neonatal mice at age of P7 to P8 were used. Basilar membrane with hair cells was dissected and bathed in external solution containing the following (in mM): 120 NaCl, 20 TEA-Cl, 2 $MgCl_2$, 2 $CoCl_2$, and 10 H-Hepes (pH 7.3 with NaOH, osmolality 300 mOsm with D-Glucose). The internal solution with the same pH and osmolality contained the following (in mM): 140 CsCl, 2 $MgCl_2$, 10 EGTA, and 10 H-Hepes. Whole-cell patch clamp was done with holding potential at 0 mV (Axon Axopatch 200B, Molecular Devices Corp.). Continuous high-resolution two-sine stimulus (390.6 and 781.2 Hz) with 10 mV peak amplitude superimposed onto a 250 ms voltage ramp (from +150 to −150 mV) was used. Data were acquired and analyzed using jClamp (Scisoft). Capacitance-voltage data were fit with two-state Boltzmann function.

$$C_m = NLC + C_{lin} = Q_{max}\frac{ze}{k_BT}\frac{b}{(1+b)^2} + C_{lin},$$

where

$$b = exp\left(-ze\frac{V_m - V_h}{k_BT}\right).$$

C_{lin} is linear membrane capacitance, Q_{max} is the maximum nonlinear charge, z is valence, e is electron charge, k_B is Boltzmann constant, T is absolute temperature, V_m is membrane potential, and V_h is voltage at peak capacitance.

Data Analysis. Each experiment contained at least three biological replicates. Data were managed and analyzed with MATLAB 2014b (MathWorks), MicroManager 1.6 software (52), Excel 2016 (Microsoft), Prism 6 (GraphPad Software), and Igor Pro-6 (WaveMetrics). All data are shown as mean ± SD, as indicated in the figure legends. We used a two-tailed *t* test for one-to-one comparison or one-way ANOVA for one-to-many comparison to determine statistical significance (*$P < 0.05$, **$P < 0.01$, ***$P < 0.001$, and ****$P < 0.0001$). Nonparametric analysis was used accordingly if the data are not in Gaussian distribution or with equal variances. N numbers are indicated in the figures. For animal tracing and locomotion evaluation, videos of mouse locomotion in open-field, footshock, and pup-retrieval test were analyzed by MATLAB software and EthoVision XT software (version 11.5, Noldus). The center of the mouse was used to draw the locomotion trace. To show the speed information, the locomotion trace was dotted every 0.5 s. For footshock behavior analysis, freezing time percentage of precue (30 s before conditional stimulus) and postcue (30 s after conditional stimulus) were analyzed to compare the effect of sound-induced freezing. For Ca^{2+} data analysis, to extract fluorescence signals, we visually identified the regions of interest (ROIs) based on fluorescence intensity. To estimate fluorescence changes, the pixels in each specified ROI were averaged (F). Relative fluorescence changes, $\Delta F/F_0 = (F - F_0)/F_0$, were calculated as Ca^{2+} signals. The hemicochlear imaging data were analyzed offline by MicroManager software and Excel software. The ROI was drawn to cover each hair cell. The fluorescence intensity of ROI was normalized to its value in the frame immediately prior to stimulation.

Data Availability. All study data are included in the article and/or supporting information.

ACKNOWLEDGMENTS. We thank Drs. Wendol Williams, Joseph Santos-Sacchi, and Dhasakumar Navaratnam for critical reading and comments; Dr. Wendol Williams for editing the manuscript; Drs. Xiaoqin Wang, Xiaoke Chen, Lei Song, Xin Liang, and members of the W.X. laboratory for helpful discussions; the Imaging Core Facility, Technology Center for Protein Sciences at Tsinghua University for assistance of using imaging instruments and software; Si Li of the Dr. Qingfeng Wu laboratory for help with RNAscope experiment; Lili Niu and Xudong Shi of the H.Z. laboratory at Shenzhen Institutes of Advanced Technology, Chinese Academy of Sciences for manufacturing the high-frequency amplifier and ultrasonic transducers; Dr. Qiuying Chen of the Dr. Guoxuan Lian laboratory at Institute of Acoustics, Chinese Academy of Sciences for manufacturing the ultrasonic transducers; and Dr. Guangzhen Xing at National Institute of Metrology for calibrating the ultrasonic transducers and the high-frequency amplifier. This work was supported by the National Natural Science Foundation of China (31522025, 31571080, 81873703, 31861163003, and 31825014), Beijing Municipal Science and Technology Commission (Z181100001518001), National Key Scientific Instrument and Equipment Development Project (81527901), and a startup fund from the Tsinghua-Peking Center for Life Sciences. W.X. is a CIBR (Chinese Institute for Brain Research) cooperative investigator (2020-NKX-XM-04) funded by the Open Collaborative Research Program of Chinese Institute for Brain Research.

1. S. L. Hopp, M. J. Owren, C. S. Evan, *Animal Acoustic Communication: Sound Analysis and Research Methods* (Springer, 1998).
2. C. V. Portfors, D. J. Perkel, The role of ultrasonic vocalizations in mouse communication. *Curr. Opin. Neurobiol.* **28**, 115–120 (2014).
3. A. Uematsu *et al*., Maternal approaches to pup ultrasonic vocalizations produced by a nanocrystalline silicon thermo-acoustic emitter. *Brain Res.* **1163**, 91–99 (2007).
4. S. R. Egnor, K. M. Seagraves, The contribution of ultrasonic vocalizations to mouse courtship. *Curr. Opin. Neurobiol.* **38**, 1–5 (2016).
5. K. R. Foster, M. L. Wiederhold, Auditory responses in cats produced by pulsed ultrasound. *J. Acoust. Soc. Am.* **63**, 1199–1205 (1978).
6. G. Ehret, B. Haack, Ultrasound Recognition in house mice—Key-stimulus configuration and recognition mechanism. *J. Comp. Physiol.* **148**, 245–251 (1982).
7. K. Ohyama, J. Kusakari, K. Kawamoto, Ultrasonic electrocochleography in guinea pig. *Hear. Res.* **17**, 143–151 (1985).
8. K. Ohyama, J. Kusakari, K. Kawamoto, Sound perception in the ultrasonic region. *Acta Otolaryngol. Suppl.* **435**, 73–77 (1987).
9. N. Suga, X. Ma, Multiparametric corticofugal modulation and plasticity in the auditory system. *Nat. Rev. Neurosci.* **4**, 783–794 (2003).
10. A. J. Hudspeth, SnapShot: Auditory transduction. *Neuron* **80**, 536.e531 (2013).
11. W. Xiong, Z. Xu, *Mechanotransduction of the Hair Cell* (Springer Singapore, 2018).
12. R. Fettiplace, K. X. Kim, The physiology of mechanoelectrical transduction channels in hearing. *Physiol. Rev.* **94**, 951–986 (2014).
13. P. G. Gillespie, U. Müller, Mechanotransduction by hair cells: Models, molecules, and mechanisms. *Cell* **139**, 33–44 (2009).
14. B. Coste *et al*., Piezo1 and Piezo2 are essential components of distinct mechanically activated cation channels. *Science* **330**, 55–60 (2010).
15. S. E. Murthy, A. E. Dubin, A. Patapoutian, Piezos thrive under pressure: Mechanically activated ion channels in health and disease. *Nat. Rev. Mol. Cell Biol.* **18**, 771–783 (2017).
16. L. Wang, *et al*., Structure and mechanogating of the mammalian tactile channel PIEZO2. *Nature* **573**, 225–229 (2019).
17. B. Xiao, Levering mechanically activated piezo channels for potential pharmacological intervention. *Annu. Rev. Pharmacol. Toxicol.* **60**, 195–218 (2020).
18. Z. Wu *et al*., Mechanosensory hair cells express two molecularly distinct mechanotransduction channels. *Nat. Neurosci.* **20**, 24–33 (2017).
19. M. Beurg, A. C. Goldring, A. J. Ricci, R. Fettiplace, Development and localization of reverse-polarity mechanotransducer channels in cochlear hair cells. *Proc. Natl. Acad. Sci. U.S.A.* **113**, 6767–6772 (2016).
20. M. Beurg, R. Fettiplace, PIEZO2 as the anomalous mechanotransducer channel in auditory hair cells. *J. Physiol.* **595**, 7039–7048 (2017).
21. C. Grimm *et al*., A helix-breaking mutation in TRPML3 leads to constitutive activity underlying deafness in the varitint-waddler mouse. *Proc. Natl. Acad. Sci. U.S.A.* **104**, 19583–19588 (2007).
22. J. R. Melcher *et al*., Generators of the brainstem auditory evoked potential in cat. I. An experimental approach to their identification. *Hear. Res.* **93**, 1–27 (1996).
23. G. Ehret, Development of absolute auditory thresholds in the house mouse (*Mus musculus*). *J. Am. Audiol. Soc.* **1**, 179–184 (1976).
24. A. M. Taberner, M. C. Liberman, Response properties of single auditory nerve fibers in the mouse. *J. Neurophysiol.* **93**, 557–569 (2005).
25. A. E. Dubin *et al*., Inflammatory signals enhance piezo2-mediated mechanosensitive currents. *Cell Rep.* **2**, 511–517 (2012).
26. S. H. Woo *et al*., Piezo2 is required for Merkel-cell mechanotransduction. *Nature* **509**, 622–626 (2014).
27. J. A. Garcia-Lazaro, K. N. Shepard, J. A. Miranda, R. C. Liu, N. A. Lesica, An overrepresentation of high frequencies in the mouse inferior colliculus supports the processing of ultrasonic vocalizations. *PLoS One* **10**, e0133251 (2015).
28. K. P. Hunter, J. F. Willott, Aging and the auditory brainstem response in mice with severe or minimal presbycusis. *Hear. Res.* **30**, 207–218 (1987).
29. Q. Y. Zheng, K. R. Johnson, L. C. Erway, Assessment of hearing in 80 inbred strains of mice by ABR threshold analyses. *Hear. Res.* **130**, 94–107 (1999).
30. T. Ohyama, A. K. Groves, Generation of Pax2-Cre mice by modification of a Pax2 bacterial artificial chromosome. *Genesis* **38**, 195–199 (2004).
31. H. Yang, X. Xie, M. Deng, X. Chen, L. Gan, Generation and characterization of Atoh1-Cre knock-in mouse line. *Genesis* **48**, 407–413 (2010).
32. D. Jing *et al*., Tissue clearing of both hard and soft tissue organs with the PEGASOS method. *Cell Res.* **28**, 803–818 (2018).
33. S. P. Peron, J. Freeman, V. Iyer, C. Guo, K. Svoboda, A cellular resolution map of barrel cortex activity during tactile behavior. *Neuron* **86**, 783–799 (2015).
34. W. Z. Zeng *et al*., PIEZOs mediate neuronal sensing of blood pressure and the baroreceptor reflex. *Science* **362**, 464–467 (2018).
35. J. Fang *et al*., Outer hair cell-specific prestin-CreERT2 knockin mouse lines. *Genesis* **50**, 124–131 (2012).
36. J. Zheng *et al*., Prestin is the motor protein of cochlear outer hair cells. *Nature* **405**, 149–155 (2000).

37. C. Li *et al*., Characterizing a novel vGlut3-P2A-iCreER knockin mouse strain in cochlea. *Hear. Res.* **364**, 12–24 (2018).
38. W. E. Brownell, C. R. Bader, D. Bertrand, Y. de Ribaupierre, Evoked mechanical responses of isolated cochlear outer hair cells. *Science* **227**, 194–196 (1985).
39. B. Kachar, W. E. Brownell, R. Altschuler, J. Fex, Electrokinetic shape changes of cochlear outer hair cells. *Nature* **322**, 365–368 (1986).
40. J. Santos-Sacchi, S. Kakehata, S. Takahashi, Effects of membrane potential on the voltage dependence of motility-related charge in outer hair cells of the guinea-pig. *J. Physiol.* **510**, 225–235 (1998).
41. B. Pan *et al*., TMC1 forms the pore of mechanosensory transduction channels in vertebrate inner ear hair cells. *Neuron* **99**, 736–753.e6 (2018).
42. P. Kazmierczak *et al*., Cadherin 23 and protocadherin 15 interact to form tip-link filaments in sensory hair cells. *Nature* **449**, 87–91 (2007).
43. Y. Kawashima *et al*., Mechanotransduction in mouse inner ear hair cells requires transmembrane channel-like genes. *J. Clin. Invest.* **121**, 4796–4809 (2011).
44. F. Di Palma *et al*., Mutations in Cdh23, encoding a new type of cadherin, cause stereocilia disorganization in waltzer, the mouse model for Usher syndrome type 1D. *Nat. Genet.* **27**, 103–107 (2001).
45. D. Z. He, S. Jia, P. Dallos, Mechanoelectrical transduction of adult outer hair cells studied in a gerbil hemicochlea. *Nature* **429**, 766–770 (2004).
46. R. M. Edge *et al*., Morphology of the unfixed cochlea. *Hear. Res.* **124**, 1–16 (1998).
47. V. Lukacs *et al*., Impaired PIEZO1 function in patients with a novel autosomal recessive congenital lymphatic dysplasia. *Nat. Commun.* **6**, 8329 (2015).
48. C. A. Haselwandter, R. MacKinnon, Piezo's membrane footprint and its contribution to mechanosensitivity. *eLife* **7**, e41968 (2018).
49. Y. R. Guo, R. MacKinnon, Structure-based membrane dome mechanism for Piezo mechanosensitivity. *eLife* **6**, e33660 (2017).
50. Z. Qiu *et al*., The mechanosensitive ion channel piezo1 significantly mediates in vitro ultrasonic stimulation of neurons. *iScience* **21**, 448–457 (2019).
51. S. Romero *et al*., Cellular and widefield imaging of sound frequency organization in primary and higher order fields of the mouse auditory cortex. *Cereb. Cortex* **30**, 1603–1622 (2020).
52. A. Edelstein, N. Amodaj, K. Hoover, R. Vale, N. Stuurman, Computer control of microscopes using microManager. *Curr. Protoc. Mol. Biol.* **Chapter 14**, Unit14.20 (2010).
53. S. Liu *et al*., TMC1 is an essential component of a leak channel that modulates tonotopy and excitability of auditory hair cells in mice. *eLife* **8**, e47441 (2019).
54. J. Geng *et al*., A plug-and-latch mechanism for gating the mechanosensitive piezo channel. *Neuron* **106**, 438–451.e6 (2020).